Cell

RNA Ligase Structures Reveal the Basis for RNA Specificity and Conformational Changes that Drive Ligation Forward

Jayakrishnan Nandakumar,[1,2,3] Stewart Shuman,[2] and Christopher D. Lima[1,*]
[1] Structural Biology Program
[2] Molecular Biology Program
[3] Training Program in Chemical Biology
Sloan-Kettering Institute, New York, NY 10021, USA
*Contact: limac@mskcc.edu
DOI 10.1016/j.cell.2006.08.038

SUMMARY

T4 RNA ligase 2 (Rnl2) and kinetoplastid RNA editing ligases exemplify a family of RNA repair enzymes that seal 3′OH/5′PO_4 nicks in duplex RNAs via ligase adenylylation (step 1), AMP transfer to the nick 5′PO_4 (step 2), and attack by the nick 3′OH on the 5′-adenylylated strand to form a phosphodiester (step 3). Crystal structures are reported for Rnl2 at discrete steps along this pathway: the covalent Rnl2-AMP intermediate; Rnl2 bound to an adenylylated nicked duplex, captured immediately following step 2; and Rnl2 at an adenylylated nick in a state poised for step 3. These structures illuminate the stereochemistry of nucleotidyl transfer and reveal how remodeling of active-site contacts and conformational changes propel the ligation reaction forward. Mutational analysis and comparison of nick-bound structures of Rnl2 and human DNA ligase I highlight common and divergent themes of substrate recognition that can explain their specialization for RNA versus DNA repair.

INTRODUCTION

Polynucleotide ligases are ubiquitous enzymes that rectify breaks in nucleic acids by joining 3′OH and 5′PO_4 termini to form a phosphodiester (Lehman, 1974). While they have been traditionally classified as either DNA ligases or RNA ligases, this schema has begun to erode as more ligases are identified and their substrate specificities are probed. For example, most DNA ligases are capable of using either DNA or RNA as the 3′OH strand, but they require that the 5′PO_4 strand be DNA (Sekiguchi and Shuman, 1997a; Sriskanda and Shuman, 1998; Pascal et al., 2004). In contrast, an RNA ligase acting at a duplex nick requires that the 3′OH strand be RNA but is indifferent to whether the 5′PO_4 strand is DNA or RNA (Nandakumar and Shuman, 2004). Thus, ligase specificity might be dictated by discrimination of A form and B form secondary structures in duplex nucleic acid on either the 3′OH or 5′PO_4 sides of a nick. This model is difficult to extend to RNA ligases that join single-stranded polynucleotide ends.

Two families of RNA ligases, named Rnl1 and Rnl2, function in the repair of "purposeful" RNA breaks. The Rnl1 family includes bacteriophage T4 RNA ligase 1 (Silber et al., 1972; Uhlenbeck and Gumport, 1982; Wang et al., 2003) and tRNA ligases of fungi and plants (Wang and Shuman, 2005; Englert and Beier, 2005). These enzymes repair single-strand breaks in tRNA anticodon loops or the coding region of specific mRNAs that are introduced by site-specific RNA endonucleases, either as part of an RNA-based antiviral response (Amitsur et al., 1987), a response to stress on the endoplasmic reticulum (Sidrauski et al., 1996), or as a means to remove introns found in many eukaryotic tRNAs (Abelson et al., 1998). The Rnl2 family includes bacteriophage T4 RNA ligase 2 and RNA editing ligases (RELs) of the kinetoplastid protozoa *Trypanosoma* and *Leishmania* (Ho and Shuman, 2002). T4 Rnl2 and RELs are proficient in sealing nicks in duplex RNAs (Blanc et al., 1999; Palazzo et al., 2003; Nandakumar et al., 2004). This property befits the functions of RELs in mRNA editing (Schnaufer et al., 2001; Simpson et al., 2003; Stuart et al., 2005), a process whereby a guide RNA (gRNA) template strand directs endonucleolytic cleavage of a noncoding pre-mRNA to expose a 3′OH primer that is either trimmed by an exonuclease or extended by UMP additions to form a nicked RNA duplex that, when sealed by REL, has acquired coding information carried by the complementary gRNA. The role of the Rnl2-like RELs in this pathway of double-strand RNA repair is analogous to that of DNA ligases in excision repair or removal of lagging-strand primers, i.e., the Rnl2 ligases and DNA ligases act at a repaired duplex nick.

The nick ligation reaction of Rnl2 entails three nucleotidyl transfer steps akin to those of DNA ligases (Figure 1). In step 1, ligase reacts with ATP to form a covalent enzyme-(lysyl-N)-AMP intermediate with release of pyrophosphate.

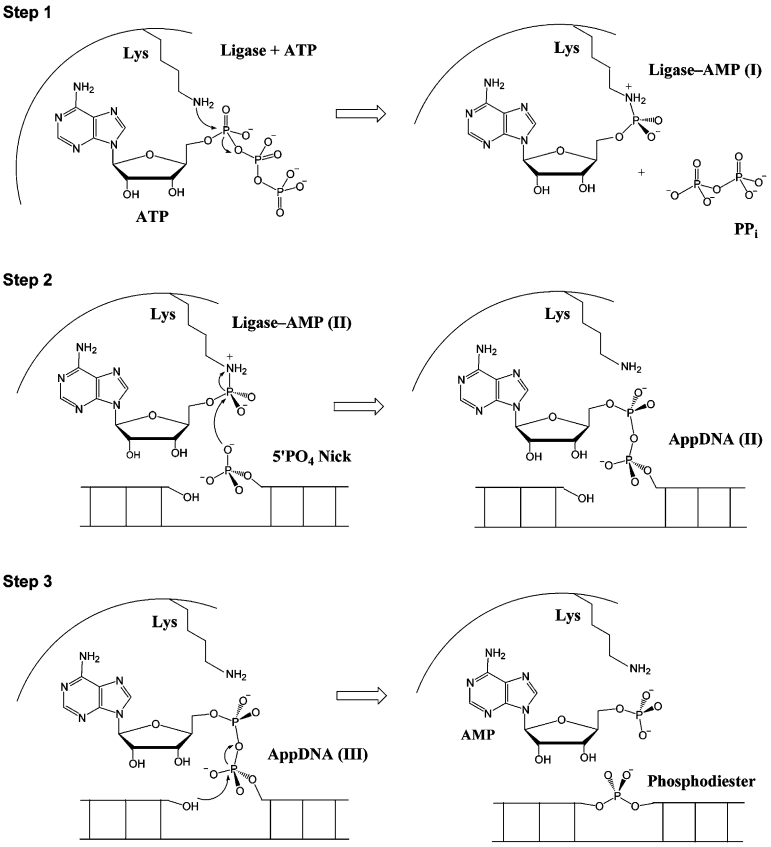

Figure 1. Three-Step Pathway of Nick Sealing by ATP-Dependent Polynucleotide Ligases

Step 1 is the attack of the active-site lysine on the α phosphorus of ATP to form a covalent ligase-AMP intermediate, releasing pyrophosphate (PP_i). Step 2 entails binding of ligase-AMP at the nick and AMP transfer to the nick 5′ phosphate to form an adenylylated nicked duplex. In step 3, the nick 3′OH attacks the nick 5′ phosphorus to form a phosphodiester, releasing AMP.

In step 2, ligase-AMP binds to the nicked duplex substrate and transfers the AMP to the 5′PO_4 terminus to form an adenylylated nicked intermediate. Ligase remains bound to the adenylylated nick and catalyzes step 3: attack of the nick 3′OH on the 5′-phosphoanhydride linkage, which results in a repaired phosphodiester and AMP release. Although steps of the nick ligation pathway of ligases are microscopically reversible when forced (Modrich et al., 1972; Sekiguchi and Shuman, 1997b), most ligases, including Rnl2, are functionally unidirectional. For example, when ligase apoenzyme reacts with a preadenylylated nicked duplex substrate, the outcome is strongly (or exclusively) biased in the direction of phosphodiester formation (forward step 3) and against deadenylylation to form ligase-AMP (reverse step 2) (Odell and Shuman, 1999; Yin et al., 2003).

It has been suggested that sealing is driven forward by remodeling the active site after each step (Odell et al., 2000; Tomkinson et al., 2006), but the repertoire of conformational switches is not well understood. Available crystal structures of DNA and RNA ligases consist mostly of single snapshots of different ligases in different functional states (Subramanya et al., 1996; Odell et al., 2000; Gajiwala and Pinko, 2004; Ho et al., 2004; Deng et al., 2004; El Omari et al., 2006; Akey et al., 2006). Only human DNA ligase I has been crystallized in a complex with DNA (Pascal et al., 2004). Nonetheless, by integrating extensive mutational data for DNA ligases with structural studies, a picture is emerging whereby the product of step 1 chemistry, designated ligase-AMP (I) in Figure 1, undergoes a large domain rotation and a conformational switch in the adenosine nucleoside that together empower nick recognition and step 2 catalysis (Shuman and Lima, 2004; Tomkinson et al., 2006). It is not known whether similar transitions occur for RNA ligases.

T4 Rnl2 is presently the best studied RNA ligase, and its properties reflect how the RELs are likely to function during mRNA editing. T4 Rnl2 and its kinetoplastid REL cousins consist of two conserved domains. The structure of their N-terminal adenylyltransferase domains are nearly identical and are similar to adenylyltransferase domains of DNA ligases (Ho et al., 2004; Deng et al., 2004). Yet Rnl2 and RELs share a unique C-terminal domain (C domain) that has no apparent sequence similarity to the OB-fold domains found at equivalent positions of all DNA ligases. The isolated adenylyltransferase domain of T4 Rnl2 is competent for catalysis of step 1 and step 3, but it is inactive in overall nick sealing and defective in binding to a nicked duplex substrate (Ho et al., 2004; Nandakumar and Shuman, 2004; 2005). The C domain is thereby implicated as critical for step 2 of the ligation pathway.

The RNA specificity of T4 Rnl2 is dictated solely by the 3′OH strand, specifically the two terminal ribonucleotides on the 3′OH side of the nick (Nandakumar and Shuman,

Table 1. Crystallographic Data and Refinement Statistics

	Rnl2-AMP	Rnl2-AppDNA/3′H/2′OH	Rnl2-AppDNA/3′OH/2′H
Protein Data Bank ID Code	2HVQ	2HVR	2HVS
Source (beamline)	NSLS X29	APS 24ID	APS 24ID
Wavelength (Å)	0.9792	0.9790	0.9797
Resolution (Å)	50.0–2.4 (2.49–2.4)	20–2.45 (2.54–2.45)	20–2.5 (2.59–2.5)
Space group	$P2_12_12_1$	$P2_12_12_1$	$P2_12_12_1$
Unit cell (Å) a, b, c	48.02, 57.85, 119.49	83.57, 106.16, 125.33	83.42, 106.74, 124.20
Number of observations	40,857	234,273	306,662
Number of reflections	12,520	41,212	38,379
Completeness (%)	91.6 (89.6)	99.0 (97.5)	98.3 (88.9)
Mean I/σI	7.4 (3.2)	17.7 (2.7)	15.6 (2.1)
R_{merge} on I[a]	12.0 (38.2)	6.6 (37.2)	7.7 (40.3)
Cutoff criteria I/σI	−1.2	0	0
Resolution limits (Å)	41.56–2.4 (2.55–2.40)	19.92–2.45 (2.60–2.45)	19.82–2.50 (2.66–2.50)
Number of reflections	12,469	41,156	38,335
Completeness (%)	91.8 (88.9)	99.0 (97.6)	98.2 (92.4)
Cutoff criteria I/σI	0	0	0
Protein/water atoms	2,520/116	5,043/129	5,043/98
Nucleic-acid atoms	—	2,006	2,006
Magnesium ions	2	—	—
Bis-Tris molecules	—	3	3
R_{cryst}[b]	21.1 (25.9)	23.6 (34.4)	23.9 (37.0)
R_{free} (5% of data)	27.4 (31.5)	29.5 (37.8)	28.3 (37.3)
Bonds (Å)/angles (°)[c]	0.006/1.2	0.007/1.2	0.007/1.1
Average B factor[d]	28.6/30.4/—/27.7	55.1/56.4/88.6/45.0	60.9/61.8/101.9/50.7

Numbers in parentheses indicate statistics for the high-resolution data bin for x-ray and refinement data.
[a] $R_{merge} = \sum hkl \sum i|I(hkl)i - <I(hkl)>|/\sum hkl \sum i <I(hkl)i>$.
[b] $R_{cryst} = \sum hkl\ |F_o(hkl) - F_c(hkl)|/\sum hkl\ |Fo(hkl)|$, where F_o and F_c are observed and calculated structure factors, respectively.
[c] Values indicate root-mean-square deviations in bond lengths and bond angles.
[d] Average B factors for main chain, side chain, nucleic acid, and water, respectively.

2004). All other nucleotides of the 3′OH strand, the 5′PO_4 strand, and the template strand can be replaced by deoxyribonucleotides without affecting nick joining activity. Transient-state kinetic analyses implicated the 2′OH of the nick in step 3 catalysis (Nandakumar and Shuman, 2005). This finding was remarkable, given that the 2′OH is not a reactant in step 3 (see Figure 1). Replacement of the 2′OH of the penultimate ribonucleoside by a 2′H caused a 50-fold reduction in Rnl2 nick-sealing activity. The basis for RNA recognition on the 3′OH side of the nick and the mechanism by which the ribose hydroxyls exert their effects remain poorly understood.

To clarify outstanding issues concerning the C domain structure, conformational transitions accompanying catalysis, and discrimination of RNA versus DNA damage, we determined crystal structures for full-length T4 Rnl2, alone and bound to duplex substrates, that capture the enzyme at multiple stages along the reaction pathway. This ensemble of structures provides new insight into the stereochemistry of nucleotidyl transfer and the changes in nucleic-acid conformation and protein/nucleic-acid contacts at the nick as the reaction proceeds.

RESULTS AND DISCUSSION

Structure of T4 Rnl2 Reveals a Unique C-Terminal Domain

The structure of full-length T4 Rnl2 (329 aa) was determined at 2.4 Å (see Experimental Procedures and Table 1). Rnl2 consists of two discrete modules: the N-terminal adenylyltransferase domain (aa 1–234) and a C-terminal domain (aa 244–329) (Figure 2A). The 9 aa segment connecting the two domains was too weak to warrant modeling. The apparent flexibility of this interdomain linker is in

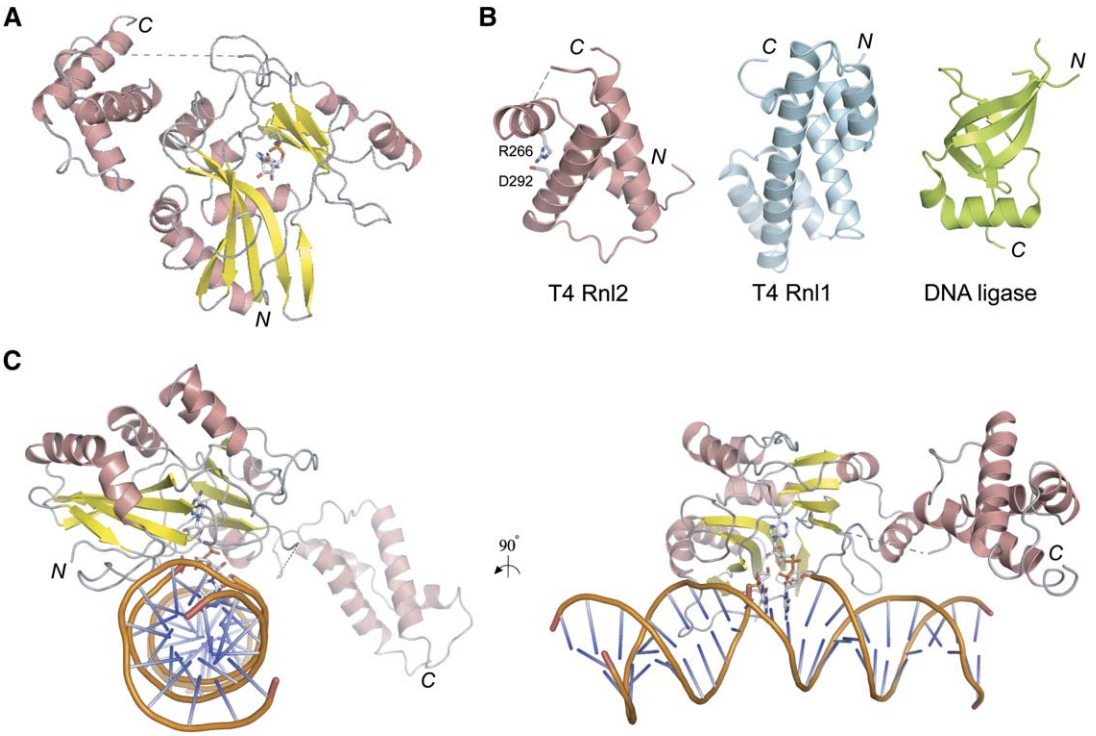

Figure 2. RNA Ligase-AMP and Ligase/Nucleic-Acid Structures

(A) Ribbon diagram of the Rnl2-AMP intermediate. The disordered amino acid linker between amino and carboxyl domains is depicted as a dashed line. N and C termini are labeled in italics.

(B) Ribbon diagrams for C-terminal domains from T4 Rnl2 (Arg266 and Asp292 shown as sticks), T4 Rnl1, and the OB-fold domain of *Chlorella* virus DNA ligase.

(C) Orthogonal views of complex A of Rnl2 at an adenylylated 3′H/2′OH nick. Graphics were prepared using PyMOL (http://pymol.sourceforge.net/).

accord with models of DNA ligase function whereby the linker acts as a fulcrum for domain movements that accompany substrate binding and reaction chemistry (Tomkinson et al., 2006). In the case of Rnl2, the C domain is reflected away from the adenylate binding pocket of the N domain so that the putative substrate-binding surface overlying the adenylate pocket is exposed.

The structure of the Rnl2 C domain consists of a four-helix bundle, has no similarity to the OB-fold domains found at the equivalent position of all known DNA ligases, and appears to be a unique and defining feature of Rnl2-like RNA ligases (Figure 2B). Although both C domains from Rnl2 and T4 Rnl1 share an all-helical structure (El Omari et al., 2006), the number of helices and topology are different (Figure 2B). A search of the Protein Data Bank using DALI (Holm and Sander, 1996) failed to identify structural homologs of the Rnl2 C domain. The fusion of three structurally divergent domains to the C terminus of adenylyltransferase domains in the Rnl2, Rnl1, and DNA ligase clades supports the proposal that ligases evolved from an undifferentiated "stand-alone" adenylyltransferase by incorporating distinct protein modules that confer biochemical specificity (Nandakumar and Shuman, 2004).

Because the primary structures of the C domains of Rnl2 and kinetoplastid RELs are conserved (Nandakumar et al., 2004), we predict that RELs share the Rnl2 C domain fold. An alanine scan of conserved residues in the C domain identified Arg266 and Asp292 as essential for activity. Elimination of either side chain abolished overall ligation of nicked duplex RNA without affecting sealing at a preadenylylated nick, i.e., R266A and D292A mutations phenocopied deletion of the C domain (Nandakumar et al., 2004). The Rnl2 crystal structure reveals that Arg266 and Asp292 form a salt bridge (Figure 2B) and are likely required for maintaining the structural integrity of the C domain.

Structure of the Covalent Rnl2-AMP Intermediate and the Mechanism of Nucleotidyl Transfer

Although Rnl2 had not been intentionally exposed to ATP or divalent cations during purification or crystallization, a composite omit map showed an AMP moiety linked covalently to Lys35-Nζ and density adjacent to the AMP phosphate that was modeled as magnesium in light of its octahedral coordination to surrounding atoms (Figure 3A; see also Figure S1A in the Supplemental Data available with this article online). Because ~50% of recombinant Rnl2 protein purified from *E. coli* is preadenylylated (Nandakumar and Shuman, 2004) and because the enzyme was never exposed to EDTA during purification

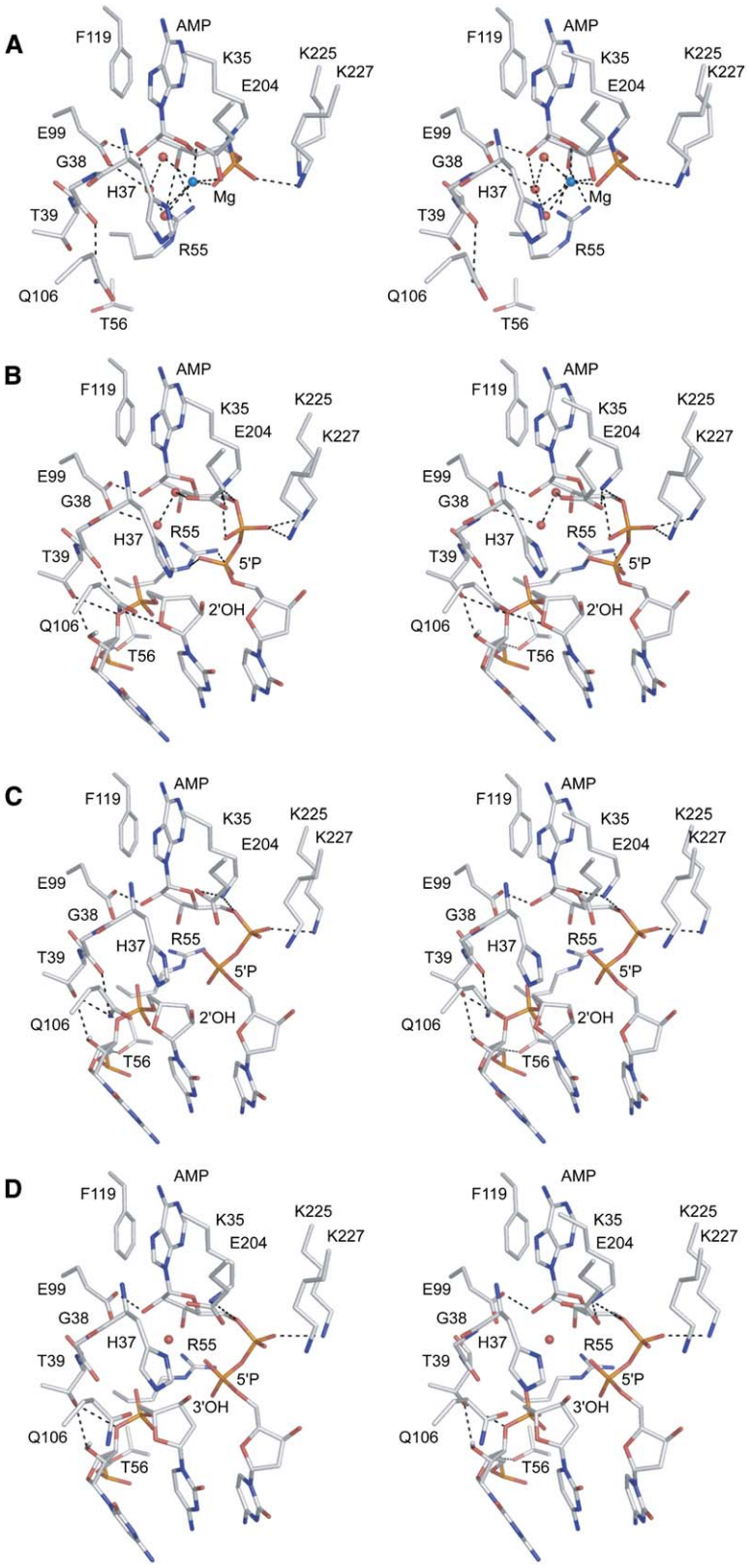

Figure 3. Serial Remodeling of Contacts in the Rnl2 Active Site in Synch with the Chemical Steps of Ligation

Stereoviews of the active sites of (A) the covalent Rnl2-AMP intermediate, (B) the A protomer of Rnl2 bound at a 3′H/2′OH nick (step 2 product), (C) the B protomer of Rnl2 bound at a 3′H/2′OH nick (step 3 substrate), and (D) Rnl2 bound at a 3′OH/2′H nick. Dashed lines depict potential hydrogen-bonding interactions. Magnesium and waters are depicted as blue and red spheres, respectively.

or crystallization, we surmise that the metal-bound Rnl2-AMP intermediate was crystallized from the mixture of Rnl2 apoenzyme and Rnl2-AMP.

The adenylate binding pocket of Rnl2 (shown in Figure 3A) is composed of side chains from the six motifs (I, Ia, III, IIIa, IV, and V) that define the nucleotidyltransferase superfamily of polynucleotide ligases and RNA capping enzymes (Shuman and Lima, 2004; Figure S5). The adenine base is stacked on Phe119 (motif IIIa), and the adenosine nucleoside is in *syn* conformation. The ribose O2′ and O3′ atoms engage in hydrogen bonds with Glu99 (motif III) and Arg55 (motif Ia), respectively. The AMP phosphate is contacted by Lys227 (motif V) and the metal ion. The magnesium ion is coordinated by Glu204 (motif IV), His37 (motif I), and two waters. The metal and each of the aforementioned side chains (except His37) are essential for the adenylylation reaction of Rnl2 with ATP (Ho and Shuman, 2002; Yin et al., 2003).

It is instructive to compare the covalent Rnl2-AMP intermediate with T4 Rnl1 bound to the unreactive analog AMPCPP (El Omari et al., 2006) (Figure 4A). The adenosine nucleosides and motif I lysines superimpose well. The Rnl1 lysine is apical to the pyrophosphate leaving group, in an optimal orientation for in-line attack on the α phosphorus. In the Rnl1-AMPCPP complex, a magnesium ion coordinates the β-phosphate and a calcium ion coordinates the α-phosphate; the latter occupies a position close to the magnesium in the Rnl2-AMP structure. Superposition of the substrate (Rnl1) and product (Rnl2) complexes indicates that the phosphorus center undergoes a stereochemical inversion during step 1 catalysis (Figure 4A). Comparison of the Rnl1-AMPCPP structure with the complex of the isolated N-terminal domain of *T. brucei* REL1 bound to ATP (Deng et al., 2004) reveals that the REL1 structure likely exemplifies an unproductive binding mode in which catalysis is precluded because the pyrophosphate leaving group is orthogonal to the lysine nucleophile (Figure S2).

Structure of Rnl2 at an Adenylylated Nicked Duplex: The Step 2 Product

Crystals were obtained for Rnl2 in the presence of a divalent cation and a 24 bp nicked duplex composed of three oligonucleotides: a 12-mer 5′PO_4 DNA strand; a 24-mer template DNA strand; and a 12-mer strand on the 3′ side of the nick consisting of ten deoxynucleotides, a penultimate 2′OMe ribonucleotide, and a terminal 3′H/2′OH nucleotide (Figure S3). This ligand was based on a minimal RNA-containing duplex that serves as an effective substrate for nick sealing by Rnl2 (Nandakumar and Shuman, 2004). 3′H modification at the nick ensures that any reaction of Rnl2 at the nick will not proceed beyond step 2. The structure of the complex was determined at 2.45 Å resolution (Table 1). The asymmetric unit contained two Rnl2/nucleic-acid complexes (Figure S3). The refined model for complex A includes Rnl2 segments 1–231 and 246–332; complex B includes segments 1–230 and 247–334. As observed in the Rnl2-AMP structure, the linker that joins the N and C domains was disordered. Rnl2 protomers in the A and B complexes can be aligned with a root-mean-square deviation (rmsd) of 2.6 Å at 317 Cα positions. Considered separately, the N domains aligned with an rmsd of 0.5 Å over 230 Cα positions, while the C domains aligned to an rmsd of 0.89 Å over 86 Cα positions. In both complexes, the active site of the adenylyltransferase domain is located over the nick (Figure 2C), whereas the C domain makes no contacts to either the adenylyltransferase domain or the duplex but is involved in crystal packing contacts with the nucleic acid of an adjacent complex (Figure S3).

A simulated annealing omit map revealed that Rnl2 had catalyzed transfer of AMP to the nick 5′PO_4 to form an adenylylated nick with continuous density over the phosphoanhydride linkage while severing the connection between Lys35 and the AMP phosphate (Figure S1B). Superposition of the adenylylated nick of complex A on the Rnl2-AMP intermediate (Figure 4B) shows that the phosphorus center of AMP undergoes inversion during catalysis of step 2, while the adenosine nucleoside remains in *syn* conformation. Because the departed Lys35 nucleophile is positioned apical to the phosphoanhydride of the newly formed AppDNA, we conclude that the structure of complex A captures Rnl2 in the state immediately after completion of step 2 chemistry. Thus, we will refer to complex A as the step 2 product, corresponding to AppDNA (II) in Figure 1.

Active-Site Remodeling between Steps 1 and 2

Figure 3B shows the Rnl2 active site in the step 2 product complex. Although magnesium was included in the enzyme/nucleic-acid mixture to promote catalysis, we did not observe electron density consistent with a metal ion in this structure, suggesting that the metal ion dissociated from the active site after completion of step 2. Comparison to the active site of the Rnl2-AMP intermediate (Figure 3A) reveals that contacts to the adenylate were remodeled during the transition through step 2. In particular, the AMP phosphate has gained contacts to Lys225 (motif V) and Lys35 (motif I), which now join Lys227 (motif V) in coordinating three of the four phosphate oxygens. Absent a metal, Glu204 (motif IV) coordinates a water and forms an ion pair with Lys35. The most significant conformational change involves Arg55 (motif Ia), which has severed its contact to the ribose O3′ (seen in Rnl2-AMP) in favor of a bidentate interaction with two nonbridging oxygens of the nick 5′PO_4 (Figure 3B and Figure 4B). This implicates Arg55 in nick recognition and orientation of the nick 5′PO_4 for nucleophilic attack on the lysyl-AMP and is consistent with mutational results showing that Arg55 is essential for step 2 (Yin et al., 2003).

Conformational Switch at the Adenylylated Nick Generates the Substrate for Step 3

Although complex B of the asymmetric unit has also undergone catalysis of step 2, the simulated annealing omit map indicates that the nick 5′ terminus adopts a

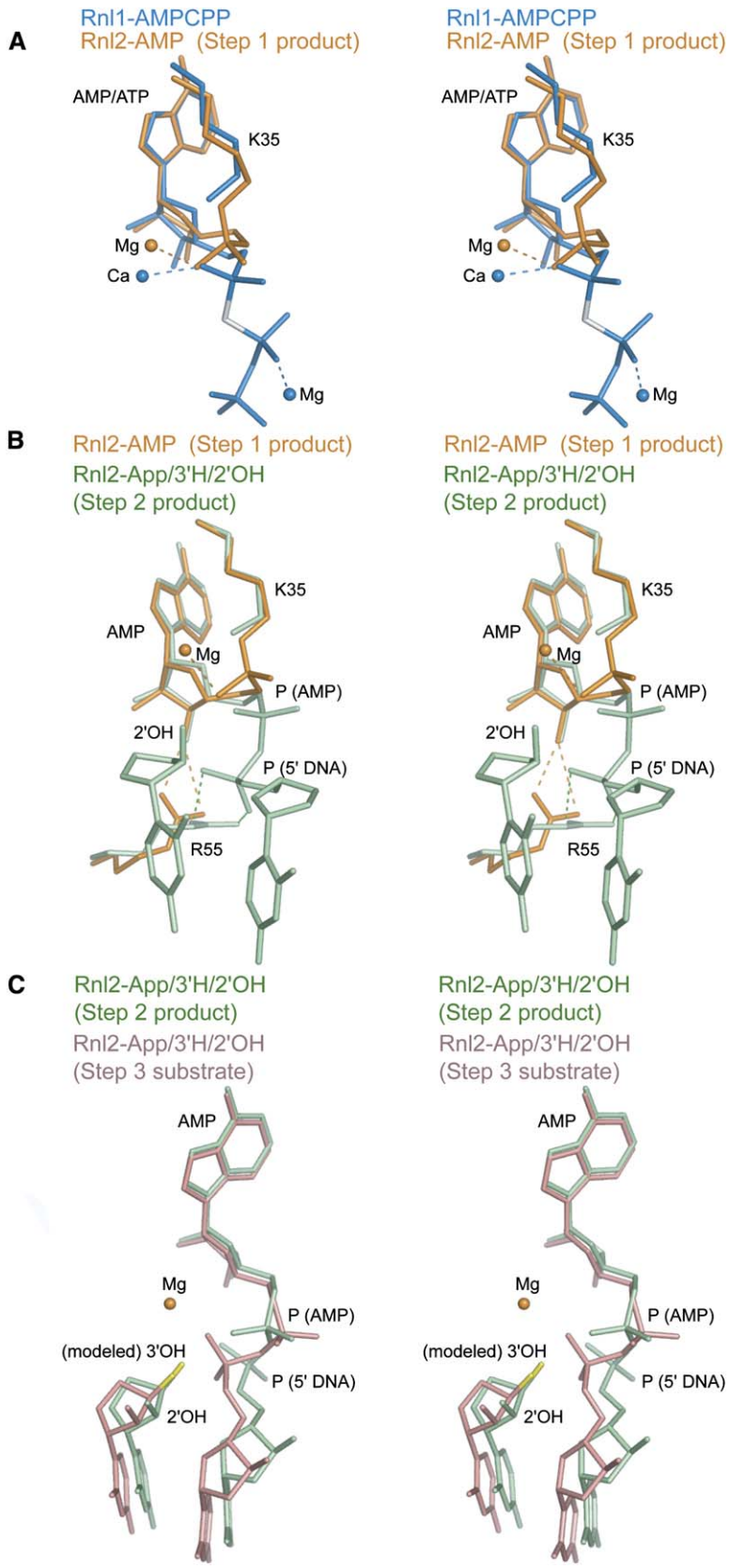

Figure 4. Stereochemistry of Nucleotidyl Transfer

(A) Superposition of T4 Rnl2 ligase-AMP (gold) on T4 Rnl1 bound to AMPPCP (blue) reveals the stereochemical inversion at the ATP α phosphorus (step 1, ligase adenylylation).

(B) Superposition of Rnl2 ligase-AMP (gold) on Rnl2 bound to a 3′H/2′OH nick (protomer A, green) reveals the stereochemical inversion at the AMP phosphorus (step 2, polynucleotide adenylylation).

(C) Superposition of structures of the A protomer (green) and B protomer (pink) of Rnl2 bound to an adenylylated 3′H/2′OH nick shows the conformational switch of the phosphoanhydride that converts the step 2 product into the step 3 substrate. A yellow atom depicts the modeled 3′OH terminus at the nick. The magnesium ion position is derived from the Rnl2-AMP structure and is shown for reference.

conformation different from that seen in the A complex (Figure S1C). The change entails rotation of the AppN pyrophosphate so that the bridging oxygen is now orthogonal to Lys35 (Figure 3C), which effectively precludes reversal of step 2 chemistry. The consequences of this change for step 3 catalysis are illustrated in Figure 4C, which shows a superposition of the adenylylated nicks of complexes A and B, with a 3′OH group modeled in lieu of the 3′H. In the step 2 product complex (in green), the nick 5′P atom is far from the nick 3′OH (3.8 Å), and the leaving bridging oxygen of AMP is positioned orthogonal to the attacking nick 3′OH. Thus, the step 2 product is unfit for catalysis of step 3. However, in the B complex (colored pink), rotation of the AppN pyrophosphate brings the 3′OH and the nick 5′P atom closer together (2.7 Å) and positions the AMP leaving group apical to the 3′OH nucleophile (Figure 4C). We conclude that the B complex captures Rnl2 in the state that mimics the enzyme immediately prior to catalysis of phosphodiester bond formation. Thus, we will refer to complex B as the step 3 substrate, corresponding to AppDNA (III) in Figure 1.

The transition from step 2 product to step 3 substrate is accompanied by another round of remodeling of the protein-nucleotide contacts in the active site (Figure 3C), whereby contacts to the AppN pyrophosphate in the step 2 product are lost in the step 3 substrate. Specifically, Arg55 relinquishes its bidentate contact to the nick 5′PO_4, Lys227 forsakes its interaction with the AMP phosphate, and Lys35 no longer contacts one of the nonbridging AMP phosphate oxygens. Loss of these contacts might facilitate rotation of the AppN pyrophosphate to achieve a more favorable conformation for step 3. The dihedral angle of 6° in the step 2 product complex suggests a strained O-P_{AMP}-O-$P_{5'PO4}$ configuration. This "eclipsing" interaction, presumably stabilized by the network of phosphate contacts to Lys35, Arg55, Lys225, and Lys227, is sterically and electrostatically unfavorable compared to the more "gauche"-like conformation observed in the step 3 substrate complex, where the O-P_{AMP}-O-$P_{5'PO4}$ dihedral angle is 41°. Thus, structures of the A and B complexes illuminate a mechanism by which active-site remodeling and conformational changes at the nick drive the ligation reaction forward.

Structural Insights into the Role of the Nick 2′OH in RNA Specificity

The 2′OH group of the 3′ ribonucleotide at the nick is not itself chemically reactive in phosphodiester bond formation, but it is required specifically for step 3 (Figure 1). Replacing the terminal nick ribonucleoside by a 2′ deoxynucleoside slows the step 3 rate constant by a factor of 30, with little effect on the step 2 rate (Nandakumar and Shuman, 2004, 2005). To determine the role of the nick 2′OH as a specificity determinant, we crystallized Rnl2 bound to a 24 bp nicked duplex containing a 3′OH/2′H deoxynucleotide on the 3′ side of the nick. In this case, we omitted a divalent cation and included EDTA in the protein/nucleic-acid mixture to preclude step 3. Under these conditions, step 2 can occur, albeit slowly, so that nearly all of the input nicks are adenylylated (Nandakumar and Shuman, 2005). Crystals of the Rnl2-3′OH/2′H complex were isomorphous to the 2′OH/3′H complex. Omit maps indicated that Rnl2 had executed AMP transfer to the nick 5′PO_4 (Figure S1D), and electron density indicated the presence of a 3′OH at the nick. In this crystal, both A and B complexes have the same conformation at the nick, corresponding to that of the step 3 substrate (Figure 3D).

The instructive difference between the Rnl2 complexes at the 3′OH/2′H versus 2′OH/3′H nicks concerns the sugar pucker. The 3′OH/2′H terminus nick has a DNA-like 2′-endo pucker (Figure 3D), whereas the 2′OH/3′H end adopts an RNA-like 3′-endo pucker (Figure 3C). The DNA-like 2′-endo pucker displaces the 3′OH from an apical orientation relative to the AMP leaving group (as modeled in Figure 4C) so that it is not well disposed for nucleophilic attack on the DNA 5′ phosphorus (Figure 3D). The fact that step 3 occurs slowly when the 2′OH is missing suggests that a terminal deoxynucleotide can, with some frequency, flip into an RNA-like pucker to facilitate catalysis. The lesson derived from the structures, that the sugar pucker is the key RNA-specificity parameter dictated by the nick 2′OH, is consistent with the observation that a 2′OMe (which favors a 3′-endo pucker) can replace the 2′OH at the nick with little impact on step 3 catalysis (Nandakumar and Shuman, 2004).

RNA Ligase Contacts the Duplex Nucleic Acid Predominantly on the 3′OH Side of the Nick

The "footprint" of the Rnl2 adenylyltransferase domain on the nucleic-acid duplex spans 13 bp centered about the nick and involves only the face of the helix from which the 5′-adenylylated terminus of the nick projects (Figure 5A and Figure S4A). Protein contacts on the 5′PO_4 side of the nick are largely restricted to the extensive network of interactions with the AppN moiety (Figure 3). Otherwise, Rnl2 makes only a few contacts with the backbone of the template strand 6 or 7 nucleotides away from the nick across the major grove on the 5′PO_4 side (Figure 5A). The majority of the protein/nucleic contacts are located on the 3′OH side of the nick, where they are arrayed across the minor groove (Figure 5A and Figure S4A). It is likely that the observed interface of the adenylyltransferase domain with the duplex faithfully reflects how Rnl2 engages its substrate for step 3 catalysis, insofar as the C domain (which is not bound to the nucleic acid in the structure) is completely dispensable for catalysis of phosphodiester bond formation at a preadenylylated nick (Nandakumar and Shuman, 2005).

Contacts to the terminal and penultimate nucleotides on the 3′OH strand of the nick are of particular interest because these nucleotides dictate Rnl2 specificity for RNA sealing. In the step 2 product, Gln106 makes a bifurcated hydrogen bond from the amide to the ribose O4′ of the terminal nucleoside and the backbone carbonyl of Gly38 (Figure 3B). Gln106 is conserved in the Rnl2/REL family, and we have shown that the Q106A mutant of Rnl2 is

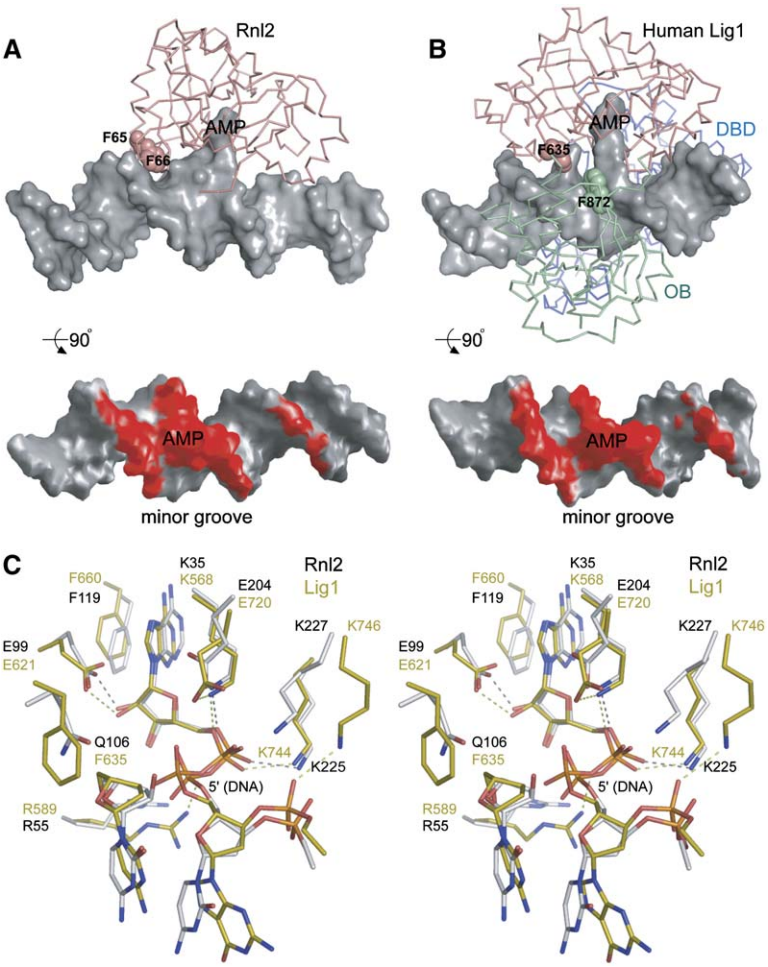

Figure 5. Comparison of Rnl2 and DNA Ligase I Engaged at Adenylylated Nicks

(A and B) Complexes of Rnl2 adenylyltransferase domain (A) and DNA ligase I (B) bound at adenylylated nicks are shown in the top panels, with nucleic acids as gray surfaces and proteins as backbone traces. Two phenylalanine residues (Phe65 and Phe66 in Rnl2; Phe635 and Phe872 in DNA Lig1) that interface with the nucleic acid are depicted by space-fill. Duplex nucleic acids are rotated ~90° in bottom panels, and proteins are omitted, so that the nick 5′ adenylate projects toward the viewer. Red surfaces contacted by the adenylyltransferase domains of Rnl2 and Lig1 were calculated with GRASP (Nicholls et al., 1991).

(C) Stereo representation of superimposed nick-bound active sites of T4 Rnl2 (protomer B, CPK) and DNA ligase I (yellow carbon atoms).

defective in overall nick sealing but competent for ligase adenylylation (Nandakumar et al., 2004). Thr56 donates a hydrogen bond from $O\gamma$ to the backbone phosphate of the penultimate nucleotide. Although Thr56 is part of nucleotidyltransferase motif Ia and is conserved as serine or threonine in most Rnl2/REL family members (Figure S5B), T56A mutation had little effect on nick joining by Rnl2 (data not shown).

Thr39 (in motif I) makes a bifurcated hydrogen bond from $O\gamma$ to the 2′OMe and 3′O of the penultimate ribonucleotide (Figure 3C and Figure 6A). The ribose sugar is critical at the penultimate position, insofar as a 2′H substitution elicits a 50-fold reduction in turnover number, whereas a 2′OMe sugar supports full ligation activity by Rnl2 (Nandakumar and Shuman, 2004). Thus, the requirement for the penultimate 2′OH is consistent with its ability to serve as a hydrogen bond acceptor, to enforce a 3′-endo pucker, or both. If the hydrogen bond from Thr39 to the ribose O2′ is the dominant factor in RNA specificity, then a T39A mutation should phenocopy a 2′H substitution on the penultimate sugar. However, T39A mutation had no effect on overall ligation activity on a nicked duplex substrate containing an all-RNA 3′OH strand at the nick (Figure 6C), suggesting that hydrogen bonding between the ribose and Thr39 is not essential for Rnl2 sealing activity. Consistent with this result, several members of the Rnl2/REL family naturally have alanine in lieu of threonine at this position (Nandakumar et al., 2004). We surmise that the RNA-like pucker is the major contribution of the 2′OH of the penultimate nucleoside.

Structural Transition of Nucleosides Flanking the Nick

The program 3DNA (Lu and Olson, 2003) was used to assess the nucleoside conformation and helical character for each nucleotide and base pair of the step 2 product (red in Figure S4C) and step 3 substrate (blue in Figure S4C). Analysis indicates that two ribonucleosides on the 3′ side of the nick and the terminal deoxynucleoside on the 5′ side adopt a 3′-endo pucker, all other deoxynucleosides of the nicked strands adopt a 2′-endo conformation (Figure S4C, left panel), and all deoxynucleosides in the template strand of the Rnl2 complexes adopt a 2′-endo pucker (Figure S4C, middle panel). Thus, sugar conformation at all positions except the 5′ deoxynucleoside of the AppN strand is correlated with the presence or

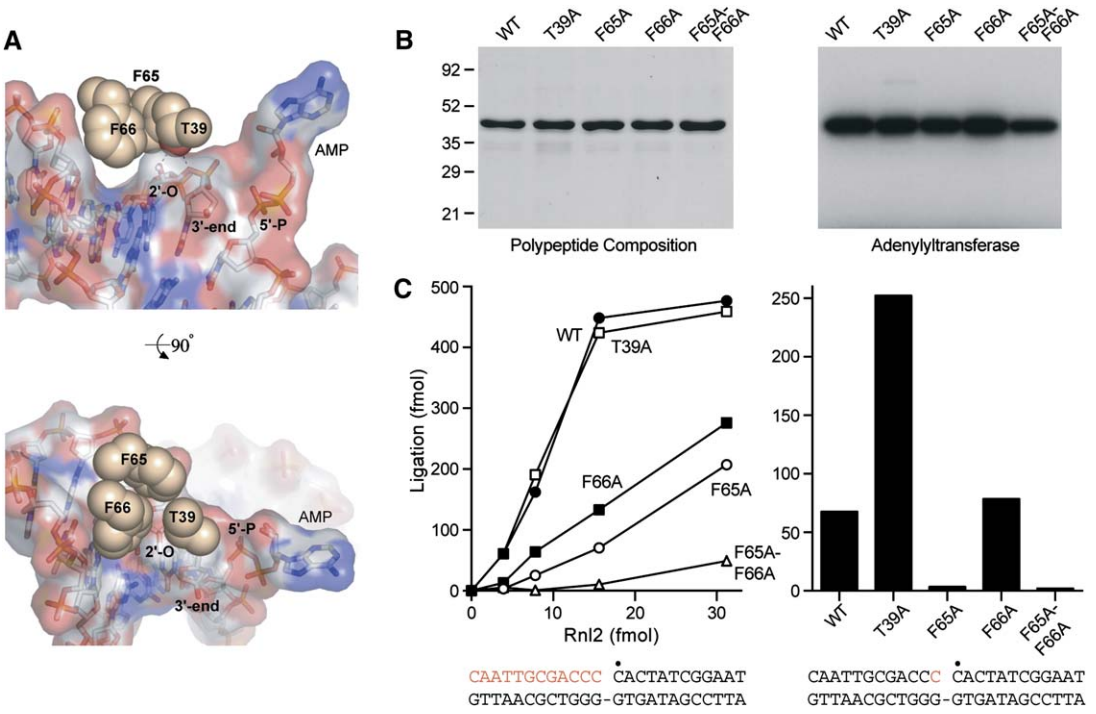

Figure 6. Mutational Analysis of Rnl2 Residues that Contact the 3′OH Side of the Nick

(A) Orthogonal views of Thr39, Phe65, and Phe66, with the surface of the duplex on the 3′ side of the nick. Phe66 penetrates the minor groove and makes van der Waals contacts to the backbone atoms of both the 3′OH and template strands.

(B) Left: Aliquots (4 μg) of the Ni-agarose preparations of wild-type Rnl2 and the indicated mutants were analyzed by SDS-PAGE. Positions and sizes (kDa) of the marker polypeptides are indicated. Right: Adenylyltransferase activity was assayed by label transfer from 20 μM [α-^{32}P]ATP to 1.25 μM wild-type or mutant Rnl2. The Rnl2-[^{32}P]AMP adduct was resolved by SDS-PAGE and visualized by autoradiography.

(C) Left: Sealing-reaction mixtures contained 500 fmol of the nicked R12 duplex (shown at bottom with the ribonucleotides in red) and wild-type or mutant Rnl2 as specified. Right: Sealing-reaction mixtures contained 500 fmol of the nicked D11R1 duplex (shown at bottom with the single ribonucleotide in red) and 63 fmol of wild-type or mutant Rnl2. • indicates the position of the [^{32}P]5′ phosphate.

absence of a 2′OH. The pucker of the furanose ring in turn affects the helical form of the duplex. The 3DNA program makes use of the Zp parameter to distinguish A and B secondary structures, and a plot of Zp values at each dinucleotide step highlighted a transition from B form to a more A-like form when approaching the nick from either end of the duplex (blue and red lines in Figure S4C, right panel). The A-like segment includes 4 base pairs flanking the nick on the 3′ side and 2 base pairs on the 5′ side.

Functional Analysis of the RNA Binding Surface

Rnl2 residues Phe65 and Phe66 project into the minor groove on the 3′ side of the nick. Phe66 makes van der Waals contacts with the ribose O2′ of the penultimate C nucleotide of the 3′ nick strand and with the sugar O3′, O4′, and C4′ atoms of the template-strand T nucleotide located across the minor groove (Figure 6A). To probe the relevance of these contacts, we produced mutated versions of Rnl2 containing F65A or F66A changes, as well as a double mutant F65A-F66A (Figure 6B). The F65A, F66A, and F65A-F66A proteins were active in ligase adenylylation (Figure 6B) but compromised to varying extents in sealing a nicked duplex with a 12-mer all-RNA 3′OH strand (referred to as an R12 nick). Whereas the F65A and F66A mutants were 16% and 30% as active as wild-type Rnl2 with the R12 substrate, the activity of the double mutant was reduced to 2% (Figure 6C, left panel). The Phe-Phe motif is conserved in viral Rnl2 homologs and in all RELs but is not present in DNA ligases. We surmise that the Phe-Phe dipeptide is a key component of the RNA-recognition surface of Rnl2-like ligases.

We considered the possibility that Rnl2 residues that contact the RNA-like segment on the 3′ side of the nick might help the enzyme discriminate between RNA and DNA, in which case the loss of such residues might actually relax the substrate specificity of Rnl2. Thus, we tested the wild-type enzyme and T39A, F65A, F66A, and F65A-F66A mutants for their ability to seal a nicked duplex that contained a single ribonucleotide at the 3′OH nick terminus (Figure 6C, right panel). This molecule (which we refer to as D11R1) is a poor substrate for sealing by wild-type Rnl2 because it lacks the critical ribose at the penultimate position of the 3′OH strand. An instructive finding was that T39A was 4-fold more active than wild-type Rnl2 in sealing the D11R1 duplex. Because T39A had no effect on sealing the R12 nick, we infer that the

presence of the threonine side chain imposes a bias against DNA on the 3′OH side by disfavoring accommodation of a B form helix near the enzyme surface. The F66A mutant was as active as wild-type Rnl2 in sealing the D11R1 nick, though this mutant was less active than wild-type Rnl2 on the R12 substrate. This result implies that Phe66, which penetrates and contacts the A form minor-groove backbone, also assists in enforcing RNA specificity. On the other hand, the F65A change was detrimental to R12 and D11R sealing (as was the F65A-F66A double mutant), signifying that Phe65 is important for forming the Rnl2 nucleic-acid binding surface illustrated in Figure 6A, but not for discriminating RNA versus DNA.

The adenylyltransferase domains of T4 Rnl2 and *T. brucei* REL1 superimpose with an rmsd of 2.3 Å for 209 equivalent C_α atoms. In addition, both Thr39 and the diphenylalanine motif are conserved in REL1. As such, our structure of Rnl2 bound at a duplex nick suggests a model whereby REL1 stabilizes the nicked mRNA/gRNA complex via interactions with the 3′OH side of the nicked RNA (Figure S5). The model places a REL-specific 27 amino acid insert between motifs III and IIIa (colored red) on the 3′OH side of the nick, where it is positioned over the template strand (analogous to the guide RNA strand in the RNA editing complex; Stuart et al., 2005).

RNA Ligase versus DNA Ligase: Further Insights into Substrate Specificity

Comparison of the structures of Rnl2 and human DNA ligase I bound at an adenylylated nick in duplex nucleic acid illuminates shared principles of the strand-sealing reactions while providing new clues to how ligases discriminate RNA versus DNA damage. Superposition of the active sites of Rnl2 (complex B) and human Lig1 at the nick indicates that the pyrophosphate linkers of the AppN termini are similarly oriented, and orthogonal to the motif I lysine, signifying that both structures correspond to a step 3 substrate complex (Figure 5C). The conserved active-site side chains and contacts to the AppN terminus are similar for both ligases. The location of the motif Ia arginine near the nick 5′PO_4 is a shared feature, underscoring the likely role of this basic residue in nick sensing during step 2. It is noteworthy that DNA Lig1 Lys746 engages the phosphate backbone at the first dinucleotide step on the 5′ side of the nick (Figure 5C); this contact does not apply in the Rnl2 structure.

Analysis of the DNA conformation of the Lig1/DNA complex underscored the important theme developed by Pascal et al. (2004): that the DNA segment flanking the nick is distorted by the bound ligase into a RNA-like conformation (Figure S4C). The A form quality and the imposition of a 3′-endo sugar pucker on the 5′ side of the nick extends 2 nucleotides further in the DNA Lig1 structure than it does in the Rnl2 structure. Most remarkably, whereas Rnl2 elicits no perturbation of the 2′-endo sugar pucker of the template-strand deoxyribonucleosides, Lig1 drives three template-strand deoxynucleosides flanking the nick into an RNA-like 3′-endo conformation (Figure S4C, middle panel).

DNA Lig1 is larger than Rnl2 and contains an N-terminal DNA binding module and a C-terminal OB-fold domain that have no counterparts in Rnl2. These domains form a clamp around the duplex DNA substrate (Figure 5B). The interface of the Lig1 adenylyltransferase domain with DNA (shown in red in Figure 5B) resembles that of Rnl2 (cf. Figure 5A) insofar as most contacts occur across the minor groove on the 3′ side of the nick. Contacts to this segment might serve to hold the 3′OH strand in place for its critical role in the step 2 polynucleotide adenylylation reaction (Yang and Chan, 1992; Odell and Shuman, 1999; Nandakumar and Shuman, 2005), a requirement that avoids adenylylation of 5′PO_4 termini that are not at nicks. Lig1 residues Phe635 and Phe872, which are located directly at the nick (Figure 5B), have been implicated in attaining the A form distortion in the Lig1/DNA structure (Pascal et al., 2004). Phe635 is uniquely conserved in DNA ligases; remarkably, it superimposes on Gln106 of Rnl2 (which contacts the nick 3′OH strand and is important for nicked RNA ligation) (Figure 5C). Phe872 is located in the OB domain of Lig1 and is conserved among DNA ligases but has no counterpart in Rnl2. It appears that DNA ligase uses the aromatic groups to promote an RNA-like configuration of the 3′ nick terminus prior to sealing (thereby accounting for the indifference of DNA ligase to whether the 3′OH strand is DNA or RNA), whereas Rnl2 (via its Phe65-Phe66 motif, Thr39, and other contacts) conforms to a pre-existing RNA-like conformation on the 3′ side of the nick. Thus, Rnl2 cannot bind productively when the 3′ strand is all DNA (Nandakumar and Shuman, 2004).

The limited interface between the Rnl2 or Lig1 adenylyltransferase domains and the 5′ side of the nick suggests that, once step 2 is completed, the enzyme/nucleic-acid complex is maintained primarily via contacts with the AMP moiety, which is covalently attached to the nick 5′PO_4, interactions that suffice for progression through step 3. Yet the DNA specificity of many DNA ligases is imposed on the 5′PO_4 side of the nick. Because many small DNA ligases consist only of the adenylyltransferase and OB domains, it is likely that DNA specificity is primarily a function of the interface of these two modules with B form nucleic acid on the 5′PO_4 side of the nick, with A form nucleic acid being unable to accommodate DNA ligase binding (Sekiguchi and Shuman, 1997a; Sriskanda and Shuman, 1998). DNA ligases I, III, and IV exhibit varying extents of discrimination against RNA, with Lig1 being most discriminatory when tested with homopolymeric (A/T) RNA/DNA hybrid substrates (Tomkinson et al., 1991; Robins and Lindahl, 1996). Pascal et al., (2004) have pointed out that the Lig1 OB fold engages in an extensive set of interactions with both DNA strands on the 5′PO_4 side of the nick that effectively measures the width of a B form DNA minor groove. Given that polyrA/polydT duplexes adopt B form structure (Gupta et al., 1985), we speculate that variations in ligase specificities might arise

due to varying sensitivities of the OB domains toward the RNA 2′OH groups in the minor groove. The Rnl2 structures captured here suggest that Rnl2 has no such mechanism to discriminate RNA versus DNA on the 5′ side of the nick, consistent with its ability to seal 5′PO_4 RNA or DNA strands.

EXPERIMENTAL PROCEDURES

T4 Rnl2 Purification

Plasmid pET-His-Smt3/Rnl2 encoded full-length T4 RNA ligase 2 fused to an N-terminal His_6-Smt3 tag; expression was driven by a bacteriophage T7 promoter (Mossessova and Lima, 2000). Cultures (8 l) of *E. coli* BL21(DE3)/pET-His-Smt3/Rnl2 were grown at 37°C to an $A_{600} \sim$ 1.0, IPTG was added to 1 mM, and incubation was continued for 3 hr. Cells were harvested by centrifugation; resuspended in 20% sucrose, 20 mM Tris-HCl (pH 7.5), 0.1 mg/ml lysozyme, 0.1% IGEPAL (Sigma), 1 mM PMSF, and 1 mM β-mercaptoethanol (BME); and lysed by sonication, and insoluble material was removed by centrifugation. His-Smt3/Rnl2 was purified by metal affinity chromatography and digested with the Smt3-specific protease Ulp1 (Mossessova and Lima, 2000) at a 500:1 ratio of Rnl2:Ulp1 during overnight dialysis in 20 mM Tris-HCl (pH 8.5), 350 mM NaCl, 1 mM BME. His-Smt3 was removed by metal affinity chromatography. Rnl2 was purified by gel filtration (Superdex 75; Pharmacia) equilibrated in 20 mM Tris-HCl (pH 8.0), 350 mM NaCl, 1 mM BME. Peak fractions were concentrated; adjusted to 10 mM Tris-HCl (pH 8.0), 100 mM NaCl, 1 mM BME; and applied to a Mono-Q anion exchange column. Rnl2 was eluted at 200 mM NaCl using a linear gradient of NaCl; concentrated to 8 mg/ml in 10 mM Tris-HCl (pH 8.0), 90 mM NaCl, 1 mM DTT; and stored at −80°C.

Rnl2 Crystallization and Structure Determination

Rnl2 crystals grew overnight at 18°C via hanging-drop vapor diffusion using a 1:1 ratio of protein:well solution (100 mM MES [pH 5.75], 10% 2-methyl-2,4-pentanediol [MPD], 30 mM NaCl). Single crystals were transferred to 100 mM MES (pH 5.75) and 20% MPD before flash freezing in liquid nitrogen. Data were processed using DENZO and SCALEPACK (Otwinowski and Minor, 1997) and CCP4 (CCP4, 1994) (Table 1). The Rnl2 N-terminal domain (aa 1–249; PDB ID code 1S68) was used for molecular replacement using MOLREP (CCP4, 1994), followed by rigid-body and all-atom refinement (REFMAC; Murshudov et al., 1997). Difference maps revealed electron density for the Rnl2 C domain, which was manually built using O (Jones et al., 1991) and refined using CNS (Brunger et al., 1998). Waters were added using ARP/wARP and manually checked using O. This model and subsequent models exhibited excellent geometry, with no residues in the disallowed regions of the Ramachandran plot.

Rnl2/Nucleic-Acid Complexes

Oligonucleotides were purchased from Oligos Etc. and purified by protein-PAK anion exchange HPLC, followed by ethanol precipitation prior to annealing. A 12-mer 5′PO_4 DNA strand (5′-pCACTATCGG AAT), a 12-mer strand (5′-CAATTGCGACCC) composed of ten deoxyribonucleotides at the 5′ end followed by a 2′OMe cytosine and terminated by a nucleotide containing either a 3′H/2′OH or a 3′OH/2′H, and a 24-mer template DNA strand (5′-ATTCCGATAGTGGGGTCGCA ATTG) were heated to 85°C in buffer containing 10 mM Tris-HCl (pH 8.0), 50 mM NaCl, and 1 mM EDTA; cooled to 22°C over 8 hr; stored at −20°C; and thawed before use. Rnl2 (180 μM) was incubated with 2 mM $MgCl_2$ and nicked 3′H/2′OH-containing substrate (180 μM) at room temperature for 20 min. Rnl2 (180 μM) was incubated with 2 mM EDTA and nicked 3′OH/2′H substrate (180 μM) on ice for 90 min. Protein/nucleic-acid complexes were mixed 1:1 with a well solution containing 100 mM Bis-Tris-HCl (pH 6.5), 22% PEG-4000, and 9% PEG-6000 at 22°C and crystallized by sitting-drop vapor diffusion. Crystals that appeared after 5–7 days were incubated at 4°C for 2 hr before transfer to 100 mM Bis-Tris-HCl (pH 6.5), 22% PEG-4000, 8% PEG-6000, and 15% ethylene glycol, followed by flash freezing in liquid nitrogen. Data were processed as described above.

Structure Determination of Rnl2-3′H/2′OH and Rnl2-3′OH/2′H Nucleic-Acid Complexes

A molecular replacement search with Rnl2(1–249) using CNS resulted in solutions for two adenylyltransferase domains in the asymmetric unit. Positions for the C domain were located using MOLREP. The model was refined by rigid-body and all-atom refinement using REFMAC. The nucleic-acid backbone, apparent in difference maps, was manually built using O and refined using REFMAC with strict NCS restraints. Final refinement was carried out using CNS without NCS restraints. The isomorphous Rnl2-3′H/2′OH complex was used as a starting model for refinement of the 3′OH/2′H nick complex using CNS. The nick 3′OH was deleted from the model prior to refinement. Difference maps and composite simulated annealing maps revealed the position of the 3′OH, which was added prior to final refinement using CNS.

Rnl2 Mutants

Alanine mutations were introduced into the pET-Rnl2 vector (Ho and Shuman, 2002) by PCR-based methods (QuikChange; Stratagene) followed by sequencing to confirm desired mutations and to exclude acquisition of unwanted coding changes. Wild-type Rnl2 and mutants T39A, F65A, F66A, and F65A-F66A were produced in *E. coli* BL21(DE3) as His_{10}-tagged fusions and purified by Ni-agarose as described (Nandakumar et al., 2004).

Enzyme Assays

Adenylyltransferase reaction mixtures (20 μl) containing 50 mM Tris-acetate (pH 6.5), 5 mM DTT, 1 mM $MgCl_2$, 20 μM [α-^{32}P]ATP, and 1.25 μM wild-type or mutant Rnl2 were incubated for 5 min at 22°C. Reactions were quenched with SDS and analyzed by SDS-PAGE. Nick-sealing reaction mixtures (10 μl) containing 50 mM Tris-acetate (pH 6.5), 40 mM NaCl, 5 mM DTT, 1 mM $MgCl_2$, 100 μM ATP, 0.5 pmol ^{32}P-labeled nicked duplex, and Rnl2 as specified were incubated for 10 min at 22°C. Reactions were quenched with EDTA/formamide. Heat-denatured mixtures were analyzed by denaturing PAGE (7 M urea/TBE), and the extent of ligation (24-mer/[12-mer + 24-mer]) was quantified by phosphorimager analysis.

Supplemental Data

Supplemental Data include five figures and can be found with this article online at http://www.cell.com/cgi/content/full/127/1/71/DC1/.

ACKNOWLEDGMENTS

This work is supported by National Institutes of Health (NIH) grants GM61906 to C.D.L. and GM63611 to S.S. C.D.L. is a Rita Allen Foundation Scholar. S.S. is an American Cancer Society Research Professor. Use of the Advanced Photon Source (APS) is supported by the US Department of Energy, Office of Science, Office of Basic Energy Sciences, under Contract No. W-31-109-Eng-38. Use of the NE-CAT beamline at Sector 24 is based upon research conducted at the Northeastern Collaborative Access Team beamlines of the APS, which is supported by award RR-15301 from the National Center for Research Resources (NCRR) at the NIH. Beamline X29A at the National Synchrotron Light Source is supported by the Office of Biological and Environmental Research and the Office of Basic Energy Sciences of the US Department of Energy and the NCRR.

Received: May 31, 2006
Revised: July 20, 2006
Accepted: August 4, 2006
Published: October 5, 2006

REFERENCES

Abelson, J., Trotta, C.R., and Li, H. (1998). tRNA splicing. J. Biol. Chem. *273*, 12685–12688.

Akey, D., Martins, A., Aniukwu, J., Glickman, M.S., Shuman, S., and Berger, J.M. (2006). Crystal structure and nonhomologous end-joining function of the ligase component of *Mycobacterium* DNA ligase D. J. Biol. Chem. *281*, 13412–13423.

Amitsur, M., Levitz, R., and Kaufman, G. (1987). Bacteriophage T4 anticodon nuclease, polynucleotide kinase and RNA ligase reprocess the host lysine tRNA. EMBO J. *6*, 2499–2503.

Blanc, V., Alfonso, J.D., Aphasizhev, R., and Simpson, L. (1999). The mitochondrial RNA ligase from *Leishmania tarentolae* can join RNA molecules bridged by a complementary RNA. J. Biol. Chem. *274*, 24289–24296.

Brunger, A.T., Adams, P.D., Clore, G.M., DeLano, W.L., Gros, P., Grosse-Kunstleve, R.W., Jiang, J.S., Kuszewski, J., Nilges, M., Pannu, N.S., et al. (1998). Crystallography & NMR system: A new software suite for macromolecular structure determination. Acta Crystallogr. D Biol. Crystallogr. *54*, 905–921.

CCP4 (Collaborative Computational Project, Number 4) (1994). The CCP4 suite: programs for protein crystallography. Acta Crystallogr. D Biol. Crystallogr. *50*, 760–763.

Deng, J., Schnaufer, A., Salavati, R., Stuart, K.D., and Hol, W.G. (2004). High resolution crystal structure of a key editosome enzyme from Trypanosoma brucei: RNA editing ligase 1. J. Mol. Biol. *343*, 601–613.

El Omari, K., Ren, J., Bird, L.E., Bona, M.K., Klarman, G., Legrice, S.F., and Stammers, D.K. (2006). Molecular architecture and ligand recognition determinants for T4 RNA ligase. J. Biol. Chem. *281*, 1573–1579.

Englert, M., and Beier, H. (2005). Plant tRNA ligases are multifunctional enzymes that have diverged in sequence and substrate specificity from RNA ligases of other phylogenetic origins. Nucleic Acids Res. *33*, 388–399.

Gajiwala, K.S., and Pinko, C. (2004). Structural rearrangement accompanying NAD+ synthesis within a bacterial DNA ligase crystal. Structure *12*, 1449–1459.

Gupta, G., Sarma, M.H., and Sarma, R.H. (1985). Secondary structure of the hybrid poly(rA).poly(dT) in solution. Studies involving NOE at 500 MHz and stereochemical modelling within the constraints of NOE data. J. Mol. Biol. *186*, 463–469.

Ho, C.K., and Shuman, S. (2002). Bacteriophage T4 RNA ligase 2 (gp24.1) exemplifies a family of RNA ligases found in all phylogenetic domains. Proc. Natl. Acad. Sci. USA *99*, 12709–12714.

Ho, C.K., Wang, L.K., Lima, C.D., and Shuman, S. (2004). Structure and mechanism of RNA ligase. Structure *12*, 327–339.

Holm, L., and Sander, C. (1996). Mapping the protein universe. Science *273*, 595–603.

Jones, T.A., Zou, J.Y., Cowan, S.W., and Kjeldgaard, M. (1991). Improved methods for building protein models in electron density maps and the location of errors in these models. Acta Crystallogr. A *47*, 110–118.

Lehman, I.R. (1974). DNA ligase: structure, mechanism, and function. Science *186*, 790–797.

Lu, X., and Olson, W.K. (2003). 3DNA: a software package for the analysis, rebuilding and visualization of three-dimensional nucleic acid structures. Nucleic Acids Res. *31*, 5108–5121.

Modrich, P., Lehman, I.R., and Wang, J.C. (1972). Enzymatic joining of polynucleotides: reversal of *Escherichia coli* deoxyribonucleic acid ligase reaction. J. Biol. Chem. *247*, 6370–6372.

Mossessova, E., and Lima, C.D. (2000). Ulp1-SUMO crystal structure and genetic analysis reveal conserved interactions and a regulatory element essential for cell growth in yeast. Mol. Cell *5*, 865–876.

Murshudov, G.N., Vagin, A.A., and Dodson, E.J. (1997). Refinement of macromolecular structures by the maximum-likelihood method. Acta Crystallogr. D Biol. Crystallogr. *53*, 240–255.

Nandakumar, J., and Shuman, S. (2004). How an RNA ligase discriminates RNA versus DNA damage. Mol. Cell *16*, 211–221.

Nandakumar, J., and Shuman, S. (2005). Dual mechanisms whereby a broken RNA end assists the catalysis of its repair by T4 RNA ligase 2. J. Biol. Chem. *280*, 23484–23489.

Nandakumar, J., Ho, C.K., Lima, C.D., and Shuman, S. (2004). RNA substrate specificity and structure-guided mutational analysis of bacteriophage T4 RNA ligase 2. J. Biol. Chem. *279*, 31337–31347.

Nicholls, A., Sharp, K.A., and Honig, B. (1991). Protein folding and association: insights from the interfacial and thermodynamic properties of hydrocarbons. Proteins *11*, 281–296.

Odell, M., and Shuman, S. (1999). Footprinting of Chlorella virus DNA ligase bound at a nick in duplex DNA. J. Biol. Chem. *274*, 14032–14039.

Odell, M., Sriskanda, V., Shuman, S., and Nikolov, D.B. (2000). Crystal structure of eukaryotic DNA ligase-adenylate illuminates the mechanism of nick sensing and strand joining. Mol. Cell *6*, 1183–1193.

Otwinowski, Z., and Minor, W. (1997). Processing of X-ray diffraction data collected in oscillation mode. Methods Enzymol. *276*, 307–326.

Palazzo, S.S., Panigrahi, A.K., Igo, R.P., Salavati, R., and Stuart, K. (2003). Kinetoplastid RNA editing ligases: complex association, characterization, and substrate requirements. Mol. Biochem. Parasitol. *127*, 161–167.

Pascal, J.M., O'Brien, P.J., Tomkinson, A.E., and Ellenberger, T. (2004). Human DNA ligase I completely encircles and partially unwinds nicked DNA. Nature *432*, 473–478.

Robins, P., and Lindahl, T. (1996). DNA ligase IV from HeLa cell nuclei. J. Biol. Chem. *271*, 24257–24261.

Schnaufer, A., Panigrahi, A.K., Panicucci, B., Igo, R.P., Salavati, R., and Stuart, K. (2001). An RNA ligase essential for RNA editing and survival of the bloodstream form of *Trypanosoma brucei*. Science *291*, 2159–2162.

Sekiguchi, J., and Shuman, S. (1997a). Ligation of RNA-containing duplexes by vaccinia DNA ligase. Biochemistry *36*, 9073–9079.

Sekiguchi, J., and Shuman, S. (1997b). Nick sensing by DNA ligase requires a 5′ phosphate at the nick and occupancy of the adenylate binding site on the enzyme. J. Virol. *71*, 9679–9684.

Shuman, S., and Lima, C.D. (2004). The polynucleotide ligase and RNA capping enzyme superfamily of covalent nucleotidyltransferases. Curr. Opin. Struct. Biol. *14*, 757–764.

Sidrauski, C., Cox, J.S., and Walter, P. (1996). tRNA ligase is required for regulated mRNA splicing in the unfolded protein response. Cell *87*, 405–413.

Silber, R., Malathi, V.G., and Hurwitz, J. (1972). Purification and properties of bacteriophage T4-induced RNA ligase. Proc. Natl. Acad. Sci. USA *69*, 3009–3013.

Simpson, L., Sbicego, S., and Aphasizhev, R. (2003). Uridine insertion/deletion RNA editing in trypanosome mitochondria: a complex business. RNA *9*, 265–276.

Sriskanda, V., and Shuman, S. (1998). Specificity and fidelity of strand joining by *Chlorella* virus DNA ligase. Nucleic Acids Res. *26*, 3536–3541.

Stuart, K.D., Schnaufer, A., Ernst, N.L., and Panigrahi, A.K. (2005). Complex management: RNA editing in trypanosomes. Trends Biochem. Sci. *30*, 99–105.

Subramanya, H.S., Doherty, A.J., Ashford, S.R., and Wigley, D.B. (1996). Crystal structure of an ATP-dependent DNA ligase from bacteriophage T7. Cell *85*, 607–615.

Tomkinson, A.E., Roberts, E., Daly, G., Totty, N.F., and Lindahl, T. (1991). Three distinct DNA ligases in mammalian cells. J. Biol. Chem. *266*, 21728–21735.

Tomkinson, A.E., Vijayakumar, S., Pascal, J.M., and Ellenberger, T. (2006). DNA ligases: structure, reaction mechanism, and function. Chem. Rev. *106*, 687–699.

Uhlenbeck, O.C., and Gumport, R.I. (1982). T4 RNA ligase. In The Enzymes, *15B*, P.D. Boyer, ed. (New York: Academic Press), pp. 31–60.

Wang, L.K., and Shuman, S. (2005). Structure-function analysis of yeast tRNA ligase. RNA *11*, 966–975.

Wang, L.K., Ho, C.K., Pei, Y., and Shuman, S. (2003). Mutational analysis of bacteriophage T4 RNA ligase 1. Different functional groups are required for the nucleotidyl transfer and phosphodiester bond formation steps of the ligation reaction. J. Biol. Chem. *278*, 29454–29462.

Yang, S.W., and Chan, J.Y.H. (1992). Analysis of the formation of AMP-DNA intermediate and the successive reaction by human DNA ligases I and II. J. Biol. Chem. *267*, 8117–8122.

Yin, S., Ho, C.K., and Shuman, S. (2003). Structure-function analysis of T4 RNA ligase 2. J. Biol. Chem. *278*, 17601–17608.

Accession Numbers

Coordinates for the crystal structures described herein have been deposited in the Protein Data Bank with the ID codes 2HVQ, 2HVR, and 2HVS.